A constitutive model based on the evolution and coalescence of elliptical micro-cracks for quasi-brittle materials

NING JianGuo, REN HuiLan[*] & FANG MinJie

State Key Laboratory of Explosion Science and Technology, Beijing Institute of Technology, Beijing 100081, China

Damage and failure of quasi-brittle materials are caused by the evolution and coalescence of micro-cracks. To solve the problem of elliptical micro-crack growth at the elastic deformation stage, a method of complex potential functions is proposed and the effect of the initial orientation on micro-crack growth and deflection is discussed. The critical stress condition for the initial damage is derived according to the criterion of micro-crack growth. Based on energy conservation during wing-crack propagation, a damage constitutive model is developed with the strain criterion created in the condition of micro-crack coalescence. The stress-strain curves of quasi-brittle materials in uniaxial compression obtained based on this model are examined with the experimental results.

micro-cracks, damage, evolution, coalescence

The elastic modulus of a material gradually decreases with increase in the number and size of micro-cracks in it during its evolution. When the number and size of micro-cracks reach a certain stage, the interactions among the cracks become very important. For example, the coalescence between cracks is a strong or nonlinear interaction occurring in the material during its fracture and failure. To obtain the strength limit under which the material fails, the nonlinear condition of coalescence between the micro-cracks must be studied.

Many experimental studies have shown that micro-crack damage was the significant features of the fracture of brittle materials [1,2]. Currently, a lot of researches focus on the growth and interaction of micro-cracks. Krajcinovic, Sumarac and Fanella [3–6], Ju and Lee [7–9] developed their micromechanical damage models for brittle materials subjected to simple axisymmetric loading by introducing the mechanism of micro-crack propagation. When subjected to tensile loading, the micro-cracks whose normal vectors approach to the stress direction of the maximum principle

will propagate first. As a rule, the fracture surface is perpendicular to the maximum tensile stress direction. However, the evolution of micro-cracks in compression becomes more complicated. Horii and Nemat-Nasser [10,11] carried out the experimental and theatrical researches, and found that micro-cracks develop in different ways, such as becoming closed, frictional sliding, intergranular propagating and kink propagating. Feng et al. [12,13] studied the damage evolution of materials by the method of the domain of micro-crack growth (DMG). Kachanov [14–16], Chudnovsky [17,18], and Gong et al. [19,20] proposed two methods, shielding and increasing the stress intensity factor, and used them to deal with the interaction between micro-cracks.

Calculating the propagation of micro-cracks depends on their structural characteristics, and the changes in which during elastic deformation cause their propagation to be affected during nonlinear deformation. Therefore, the evolution of micro-cracks during elastic deformation should be taken into consideration before their propagation and coalescence. The coalescence is the direct cause of the material's fracture. The critical propagation length of micro-cracks

---

*Corresponding author (email: huilanren@bit.edu.cn)

in many damage models [21–23] is taken as a control parameter of fracture criterion and its value calculated by the condition of coalescence is of physical significance.

In order to facilitate mathematic treatment, the elliptical micro-cracks in a quasi-brittle material are considered elliptical in this work. The evolution under planar principal stress is solved using a complex potential function. The critical stress of wing crack initiation is calculated by the micro-crack propagation criteria. Then, the constitutive relation during micro-crack propagation is developed based on the energy conservation principle. With the condition of micro-crack coalescence, the micro-crack propagation length is derived and used to calculate the fracture strain of material.

1 Growth of elliptical micro-crack

Figure 1 shows the schematic of the stress state of a representative unit containing an elliptical micro-crack. The representative unit is subjected to a far-field loading $\tilde{\sigma} = \sigma_1 \bar{e}_{x'} \bar{e}_{x'} + \sigma_2 \bar{e}_{y'} \bar{e}_{y'}$. The length of the elliptical micro-crack is $2a_0$ in its long axis and $2b_0$ in its short axis, where $b_0 = \rho a_0$ and $0 < \rho < 1$. Its orientation is at an angle of β with the direction of loading σ_1.

To study the growth of the elliptical micro-crack in the continuum medium subjected to tensile stress, for simplicity, the local coordinate system is converted into the elliptic coordinate system with the following relations:

$$\begin{cases} x = c \cosh \eta \cos \theta, & \theta \in [0, 2\pi), \\ y = c \sinh \eta \sin \theta, & \eta \in [\eta_0, +\infty), \end{cases} \quad (1)$$

where $c = \dfrac{a_0}{\cosh \eta_0} = \dfrac{b_0}{\sinh \eta_0}$, the boundary of the elliptical micro-crack is given by $\eta = \eta_0$, $\eta_0 = \operatorname{arctanh} \rho$. $\eta \to +\infty$ corresponds to $x^2 + y^2 \to +\infty$. Assuming that $\xi = \eta + i\theta$, then $z = c \cosh \xi$.
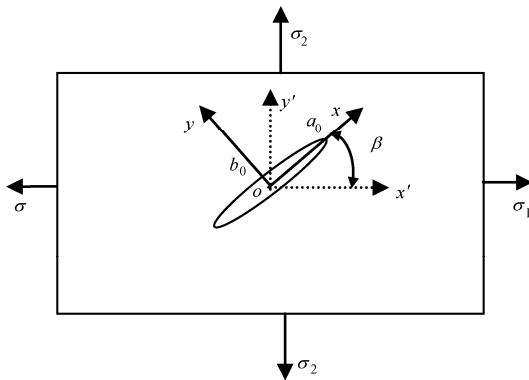

Figure 1 Schematic of the size and orientation of an elliptical micro-crack.

The boundary value of elliptical micro-crack subject to plan stress in an elastic continuum is solved by the method of complex potential function. The stress and displacement fields satisfying eq. (2) are the solutions:

$$\begin{cases} \sigma_x + \sigma_y = 4 \operatorname{Re} \psi'(z), \\ \sigma_y - \sigma_x + 2i\tau_{xy} = 2\left[\bar{z} \psi''(z) + \chi''(z) \right], \\ 2G_0 \left(u_x + iu_y \right) = \left[\dfrac{3 - v_0}{1 + v_0} \bar{\psi}(\bar{z}) - \bar{z} \psi'(z) - \chi'(z) \right], \\ 4 \operatorname{Re} \psi'(z) = \sigma \quad x^2 + y^2 \to \infty, \\ 2\left[\bar{z} \psi''(z) + \chi''(z) \right] = -\sigma \quad x^2 + y^2 \to \infty, \end{cases} \quad (2)$$

where $\psi(z)$ and $\chi(z)$ are complex functions.

$$\begin{aligned} \left(u_x + iu_y \right) = &\frac{c}{8G_0} (\sigma_1 + \sigma_2) f_1(\xi) \\ &+ \frac{c}{8G_0} (\sigma_1 - \sigma_2) \left[f_2(\xi) + f_3(\xi) + f_4(\xi) \right], \end{aligned} \quad (3)$$

where

$$f_1(\xi) = \frac{3 - v_0}{1 + v_0} \sinh \xi - |\cosh \xi|^2 \frac{1}{\sinh \xi} - \frac{\cosh 2\eta_0}{\sinh \xi},$$

$$f_2(\xi) = \frac{3 - v_0}{1 + v_0} \left(e^{2\eta_0} \cos 2\beta \cosh \xi - e^{2\eta_0 - 2i\beta} \sinh \xi \right),$$

$$f_3(\xi) = -\cosh \bar{\xi} \left(e^{2\eta_0} \cos 2\beta - e^{2\eta_0 + 2i\beta} \coth \xi \right),$$

$$f_4(\xi) = -\left[\frac{\cos 2\beta}{\sinh \xi} + e^{2\eta_0} \frac{\sinh 2(\eta_0 + i\beta - \xi)}{\sinh \xi} \right].$$

Let $\xi = \eta_0$, and the displacement at the tip of the long axis of the elliptical micro-crack is obtained:

$$u_{ax} = \frac{c}{8G_0} \left[(\sigma_1 + \sigma_2) g_1 + (\sigma_1 - \sigma_2) g_2 \right], \quad (4)$$

$$u_{ay} = \frac{c}{8G_0} (\sigma_1 - \sigma_2) g_3, \quad (5)$$

where

$$g_1 = \frac{4}{1 + v_0} \sinh \eta_0 - \frac{2 \cosh^2 \eta_0}{\sinh \eta_0},$$

$$g_2 = \left(\frac{3 - v_0}{1 + v_0} e^{\eta_0} - \cosh \eta_0 e^{2\eta_0} + \frac{e^{2\eta_0} \cosh^2 \eta_0 - 1}{\sinh \eta_0} \right) \cos 2\beta,$$

$$g_3 = \frac{4}{1 + v_0} e^{2\eta_0} \sinh \eta_0 \sin 2\beta.$$

Let $\xi = \eta_0 + i\dfrac{\pi}{2}$, and the displacement at the tip of the short axis of the elliptical micro-crack is described by

$$u_{bx} = \frac{c}{8G_0} (\sigma_1 - \sigma_2) k_1, \quad (6)$$

$$u_{by} = \frac{c}{8G_0} \left[(\sigma_1 + \sigma_2) k_2 + (\sigma_1 - \sigma_2) k_3 \right], \quad (7)$$

where

$$k_1 = \left(-\frac{3-v_0}{1+v_0}\cosh\eta_0 + \sinh\eta_0 \tanh\eta_0\right)e^{2\eta_0}\sin 2\beta,$$

$$k_2 = \frac{3-v_0}{1+v_0}\cosh\eta_0 + \frac{\sinh^2\eta_0}{\cosh\eta_0} + \frac{\cosh 2\eta_0}{\cosh\eta_0},$$

$$k_3 = \left[-\frac{3-v_0}{1+v_0}e^{\eta_0} + e^{2\eta_0}\sinh\eta_0\left(1-\tanh\eta_0\right)\right]\cos 2\beta.$$

After the elastic deformation, the lengths of the long and short half shafts of the elliptical micro-crack, respectively, become

$$a = \sqrt{\left(a_0+u_{ax}\right)^2+u_{ay}^2}, \tag{8}$$

$$b = \sqrt{u_{bx}^2+\left(b_0+u_{by}\right)^2}. \tag{9}$$

And the deflection angle of the elliptical micro-crack is expressed by the deflection angle α of the long axis:

$$\mathrm{tg}\,\alpha = \frac{\dfrac{c}{8G_0}\left(\sigma_1-\sigma_2\right)g_3}{a_0+\dfrac{c}{8G_0}\left[\left(\sigma_1+\sigma_2\right)g_1+\left(\sigma_1-\sigma_2\right)g_2\right]}. \tag{10}$$

Take an example of uniaxial loading, where $\sigma_2 = 0$. According to eqs. (4)–(10), the relative growth rates of the long half shaft, short half shaft, and the deflection angle of the elliptical micro-crack can be obtained, respectively, as shown in Figures 2 and 3.

From Figure 2 it is clear that (i) under uniaxial tensile stress, the growth rate of the short half shaft is larger than that of the long half shaft, which reveals that the ellipticity of the micro-crack changes after elastic deformation; (ii) the growth rate of the long half shaft, $R(a)=\dfrac{a-a_0}{a_0}$, decreases with the initiate angel β increasing, when β is equal to,
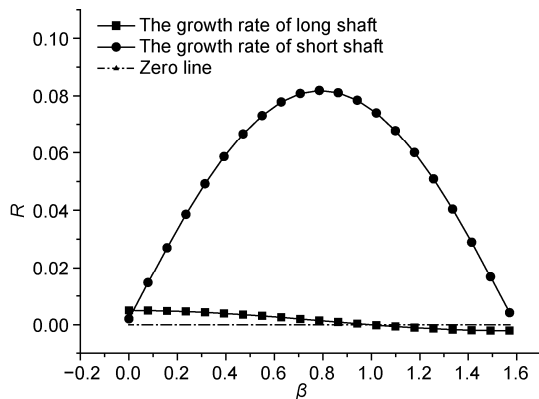
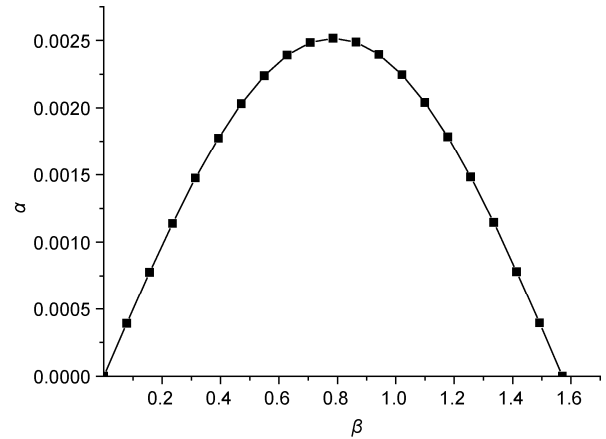**Figure 2**   Relation of growth rate of elliptical micro-crack to initial orientation.

Figrue 3   Relation of deflection angle of elliptical micro-crack to initial orientation.

further bigger than $\pi/2$, the growth rate of the long half shaft gets minimum and negative; (iii) the growth rate of the short half shaft, $R(b)=\dfrac{b-b_0}{b_0}$, varies parabolically with β, it reaches its maximum at $\beta=\pi/4$, and when the ellipticity reaches maximum, so does it, too.

Furthermore, a small deflection occurs after the elastic deformation of the elliptical micro-crack. As seen in Figure 3, at $\beta=\pi/4$, the deflection angle reaches the maximum, 0.144°, so small that it can be negligible.

2   Propagation of wing crack

2.1   Critical stress of wing crack propagation

Micro-crack propagation is the comprehensive result. It is affected by the external loading, the size of micro-crack, and the shape of micro-crack. When the stress intensity factor at its tip satisfies the crack propagation criterion, a wing crack grows from the tip in a certain direction, which will result in the nonlinear deformation of a quasi-brittle material.

The criterion of micro-crack propagation is written by

$$\left(\frac{K_{\mathrm{I}}}{K_{\mathrm{IC}}}\right)^2+\left(\frac{K_{\mathrm{II}}}{K_{\mathrm{IIC}}}\right)^2=1, \tag{11}$$

where

$$K_{\mathrm{I}} = \frac{1}{4}\left(\sqrt{\pi\rho}-2\sqrt{\pi a}\right)\left[\left(\sigma_1+\sigma_2\right)+\left(\sigma_1-\sigma_2\right)\cos 2\beta\right], \tag{12}$$

$$K_{\mathrm{II}} = \frac{1}{2}\sqrt{\pi a}\sin 2\beta\left(\sigma_1-\sigma_2\right). \tag{13}$$

The critical stress of micro-crack propagation under different kinds of loadings can be calculated by eqs. (11)–(13). In the case of uniaxial loading, that is, $\sigma_2 = 0$, eq. (11) be-

comes

$$\frac{\sigma_1^2 \pi \left(\sqrt{\rho} - 2\sqrt{a} \right)^2 \left(1 + \cos 2\beta \right)^2}{16 K^2_{\text{IC}}} + \frac{\sigma_1^2 \pi a \sin^2 2\beta}{4 K^2_{\text{IIC}}} = 1, \quad (14)$$

where a is a function of σ_1. The critical stress of elliptical micro-crack propagation can be obtained by solving eq. (14) through $\sigma = \sigma_{\text{cr}}$.

Figure 4(a) shows the variation of the critical stress versus the initial orientation β of the elliptical micro-crack. From the figure it is obvious that (i) the critical stress tends to infinity when $\beta = 0$, meaning the micro-crack whose orientation parallels the loading direction will not propagate; (ii) the critical stress decreases with β increasing and tends to the stable value, 0.27 GPa, in the range $\pi/4 \leqslant \beta \leqslant \pi/2$, which indicates that micro-crack propagation occurs mostly in the range $\pi/4 \leqslant \beta \leqslant \pi/2$. Figure 4(b) shows the variation of the critical stress versus the initial size of the elliptical micro-crack. From the figure it is clear that the larger the initial size of the micro-crack is, the smaller the critical stress of wing crack propagation, meaning material will go into the damage stage under smaller loadings.
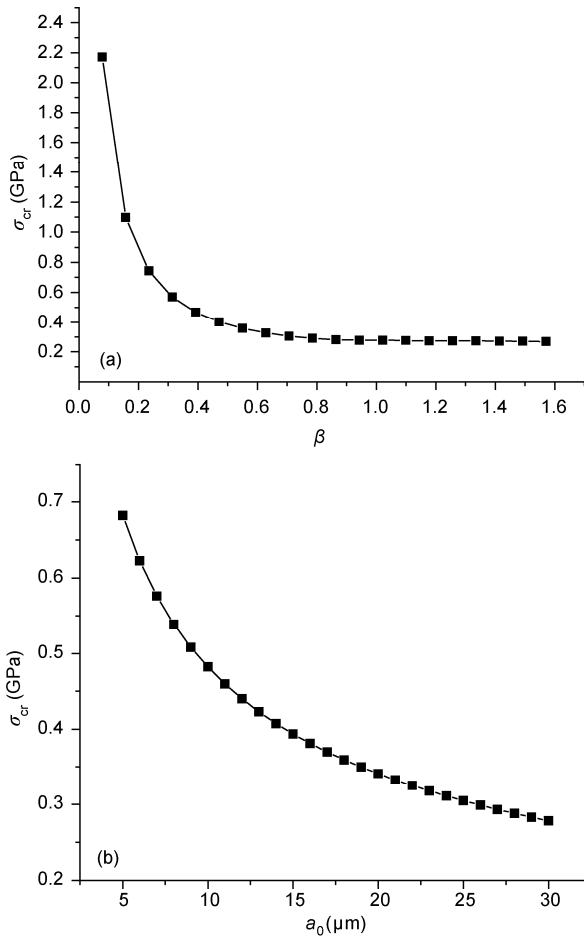

Figure 4 Relations of critical stress to initial orientation (a) and initial size (b).

2.2 Direction of wing crack propagation

In the fracture analysis of rocks and other brittle materials, the criterion of maximum circumferential stress is often used to determine the wing crack propagation direction. It states that a wing crack initiates and grows at the micro-crack tip in the direction of the maximum circumferential stress when the circumferential stress reaches a critical value. The circumferential stress at the tip of the elliptical micro-cracks in the ϑ direction is

$$\sigma_{\vartheta} = \frac{1}{\sqrt{2\pi r}} \cos \frac{\vartheta}{2} \left(K_{\text{I}} \cos^2 \frac{\vartheta}{2} - \frac{3}{2} K_{\text{II}} \sin \vartheta \right), \quad (15)$$

where K_{I} is termed as the stress intensity factor in the directions ϑ, and

$$K_{\text{I}}(\vartheta) = K_{\text{I}} \cos^3 \frac{\vartheta}{2} - \frac{3}{2} K_{\text{II}} \sin \vartheta \cos \frac{\vartheta}{2}. \quad (16)$$

The direction of the maximum circumferential stress should satisfy the following equations:

$$\begin{cases} \dfrac{\partial K_{\text{I}}(\vartheta)}{\partial \vartheta} = 0, \\ \dfrac{\partial^2 K_{\text{I}}(\vartheta)}{\partial^2 \vartheta} < 0. \end{cases} \quad (17)$$

Then, the equation with respect to the initial angle of wing crack propagation, ϑ_0, is obtained as

$$K_{\text{I}} \sin \vartheta_0 + K_{\text{II}} \left(3 \cos \vartheta_0 - 1 \right) = 0, \quad (18)$$

2.3 Effective compliance tensor of damaged material

In the elastic deformation stage, micro-cracks only deform the surrounding material in which they exist, but do not induce its damage. However, when wing cracks initiate at the tips of elliptical micro-cracks, the material instantaneously goes into the damage stage.

Assume that the elliptical micro-cracks are ideally uniform distributed in the material, that is, each micro-crack has the same shape, size, and spacing. By the sparse distribution method, the components of the effective compliance tensor are calculated as follows:

$$\overline{S}_{1111} = \frac{1}{E_0} + \frac{f}{E_0} \left[\frac{2+\rho}{\rho} \sin^4 \beta + \left(2\rho + 1 \right) \cos^4 \beta \right.$$
$$\left. + \frac{\left(1 + \rho \right)^2}{2\rho} \sin^2 2\beta - \frac{\sin^2 2\beta}{2} \right],$$

$$\overline{S}_{1122} = -\frac{v_0}{E_0} - \frac{f}{E_0} \left[-\frac{1}{2} \sin^2 2\beta - \left(\cos^4 \beta + \sin^4 \beta \right) \right],$$

$$\overline{S}_{2222} = \frac{1}{E_0} + \frac{f}{E_0} \left[\frac{2+\rho}{\rho} \cos^4 \beta + \left(2\rho + 1 \right) \sin^4 \beta \right.$$

$$+\frac{(1+\rho)^2}{2\rho}\sin^2 2\beta-\frac{\sin^2 2\beta}{2}\Bigg],\tag{19}$$

$$\bar{S}_{1212}=\frac{1+v_0}{E_0}+\frac{f}{E_0}\frac{(\rho+1)^2\sin^2 2\beta}{2\rho},$$

where $f=n_a\pi\rho a^2$, and n_a is the number of micro-cracks per unit area.

2.4 Nonlinear constitutive model

Figure 5 shows that wing crack propagation will cause the damaged material to be damaged further. According to the energy balance principle, the work, *W*, done by the loading when the wing crack length reaches *l* is equal to the elastic strain energy, that is

$$W=2U_e.\tag{20}$$

The elastic strain energy released in the process of wing crack propagating can be obtained by integrating the energy releasing rate, *G(l)*, within the wing crack length, *l*, as

$$U_e=2\int_0^l G(l)\mathrm{d}l,\tag{21}$$

where *G(l)* is defined as

$$G(l)=\frac{(\kappa_0+1)(1+v_0)}{4E_0}\left(K_{\mathrm{I}}^2+K_{\mathrm{II}}^2\right),\tag{22}$$

where K_{I} and K_{II} are called the stress intensity factors driving the wing crack to grow to the length of *l*, respectively. They are given by [21]

$$K_{\mathrm{I}}=\frac{2a\tau\cos\vartheta}{\sqrt{\pi(l+l^*)}}+\sigma_n^l\sqrt{\pi l},\tag{23}$$

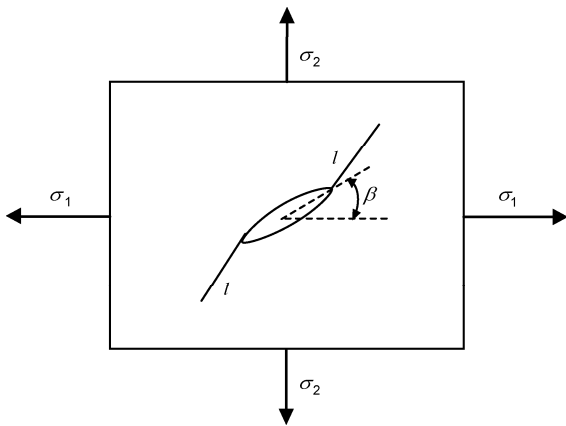$$K_{\mathrm{II}}=\frac{2a\tau\sin\vartheta}{\sqrt{\pi(l+l^*)}},\tag{24}$$

Figure 5   Schematic diagram of wing crack growth.

where

$$\tau=(\sigma_1-\sigma_2)\cos\beta\sin\beta,\tag{25}$$

$$\sigma_n^l=\frac{1}{2}\Big[(\sigma_1+\sigma_2)+(\sigma_1-\sigma_2)\cos 2(\beta+\vartheta)\Big].\tag{26}$$

For plane stress, $\kappa_0=(3-v_0)/(1+v_0)$. The crack length l^* has been introduced, so let *l*=0, and the stress intensity factors are accurately calculated by eqs. (23) and (24), l^*=0.27*a*.

By substituting eqs. (22)–(26) into eq. (21), the elastic strain energy can be obtained:

$$U_e=\frac{(\kappa_0+1)(1+v_0)}{2E_0}\Bigg[\frac{4a^2\tau^2}{\pi}\ln\left(\frac{l+l^*}{l^*}\right)$$
$$+4a\tau\sigma_n^l l\cos\vartheta+\left(\sigma_n^l\right)^2\pi\frac{l^2}{2}\Bigg].\tag{27}$$

Thus, the total work done by the loadings, σ_1 and σ_2, is

$$W=(\sigma_1\Delta\varepsilon_1+\sigma_2\Delta\varepsilon_2),\tag{28}$$

where $\Delta\varepsilon_1$ and $\Delta\varepsilon_2$ are the small increments of ε_1 and ε_2 acting upon each propagating wing crack in the directions, *ox′* and *ox′*, respectively.

The linear relation between the strains, $\Delta\varepsilon_1$ and $\Delta\varepsilon_2$, acted on the effective medium and the applied stress is

$$\begin{pmatrix}\Delta\varepsilon_1\\\Delta\varepsilon_2\end{pmatrix}=\begin{bmatrix}S_{11}&S_{12}\\S_{12}&S_{22}\end{bmatrix}\begin{pmatrix}\sigma_1\\\sigma_2\end{pmatrix},\tag{29}$$

where S_{ij} is the element of the compliance tensor applied upon single micro-crack. Eq. (28) can be rewritten as

$$W=\left(S_{11}\sigma_1^2+2S_{12}\sigma_1\sigma_2+S_{22}\sigma_2^2\right).\tag{30}$$

With the combination of eqs. (20), (27) and (30), the elements, S_{11}, S_{12} and S_{22} are obtained by comparing the correspondent coefficients of quadratic terms as follows:

$$S_{11}=\frac{(\kappa_0+1)(1+v_0)}{2E_0}(A+B+C+D),$$

$$S_{12}=-\frac{(\kappa_0+1)(1+v_0)}{2E_0}(A+B-E),$$

$$S_{22}=\frac{(\kappa_0+1)(1+v_0)}{2E_0}(A+B-C+F),$$

where *A*, *B*, *C*, *D*, *E*, and *F* are respectively given as

$$A=\frac{a^2\sin^2 2\beta}{\pi}\ln\left(\frac{l+l^*}{l^*}\right),$$

$$B=al\sin 2\beta\cos\vartheta\cos 2(\beta+\vartheta),$$

$$C=al\sin 2\beta\cos\vartheta,$$

$$D=\frac{\pi l^2}{8}\Big[\cos 2(\beta+\vartheta)+1\Big]^2,$$

$$E = \frac{\pi l^2}{8} \sin^2 2(\beta + \vartheta),$$

$$F = \frac{\pi l^2}{8} \left[1 - \cos 2(\beta + \vartheta) \right]^2.$$

Let the number density of micro-cracks be n_a, then the nonlinear strain caused by all the micro-cracks propagation is $n_a \begin{pmatrix} \Delta\varepsilon_1 \\ \Delta\varepsilon_2 \end{pmatrix}$, and whole strain is given by

$$\begin{pmatrix} \varepsilon_1 \\ \varepsilon_2 \end{pmatrix} = \begin{pmatrix} \overline{S}_{1111} & \overline{S}_{1122} \\ \overline{S}_{1122} & \overline{S}_{2222} \end{pmatrix} \begin{pmatrix} \sigma_1 \\ \sigma_2 \end{pmatrix} + n_a \begin{pmatrix} S_{11} & S_{12} \\ S_{12} & S_{22} \end{pmatrix} \begin{pmatrix} \sigma_1 \\ \sigma_2 \end{pmatrix}. \quad (31)$$

The nonlinear stress-strain relation during the process of micro-crack propagation is

$$\varepsilon_1 = \left(\overline{S}_{1111} + n_a S_{11} \right) \sigma_1 + \left(\overline{S}_{1122} + n_a S_{12} \right) \sigma_2, \quad (32)$$

$$\varepsilon_2 = \left(\overline{S}_{1122} + n_a S_{12} \right) \sigma_1 + \left(\overline{S}_{2222} + n_a S_{22} \right) \sigma_2. \quad (33)$$

3 Coalescence of micro-cracks

The growth of micro-cracks and propagation of wing cracks lead to nonlinear decrease in the effective elastic modulus. However, the coalescence among adjacent micro-cracks during crack propagation, accounts for the failure of the material. There are two modes of interconnection among micro-cracks, the connection between two wing cracks and the connection between wing crack and initial crack, as shown in Figure 6. With the same micro-crack spacing, the connection between two wing cracks is the case where the connection occurs as the crack propagates the shortest length, which occurs, of course, in a lower strength of material.

Figure 7 schematically shows that only those adjacent wing cracks with the same propagating direction can be connected together. The coalescence of two wing cracks needs to satisfy eq. (34). If the spacing between the two cracks in one direction is known, the other spacing between them in another direction can be obtained by

$$w_1 = \operatorname{ctan}(\vartheta + \beta)(w_2 - a \sin\beta) + a \cos\beta. \quad (34)$$

When wing cracks coalescence occurs in some rock or quasi-brittle material subject to strain ε, their propagation length is

$$l = \frac{2w_2 - 2a \sin\beta}{\sin(\vartheta + \beta)}. \quad (35)$$

Thus, the relation between the propagation length l and strain ε_i can be written as

$$\varepsilon_i = \frac{l}{v_{cm}} \dot{\varepsilon} + \varepsilon_i^{\mathrm{cr}} \quad (i = 1, 2), \quad (36)$$
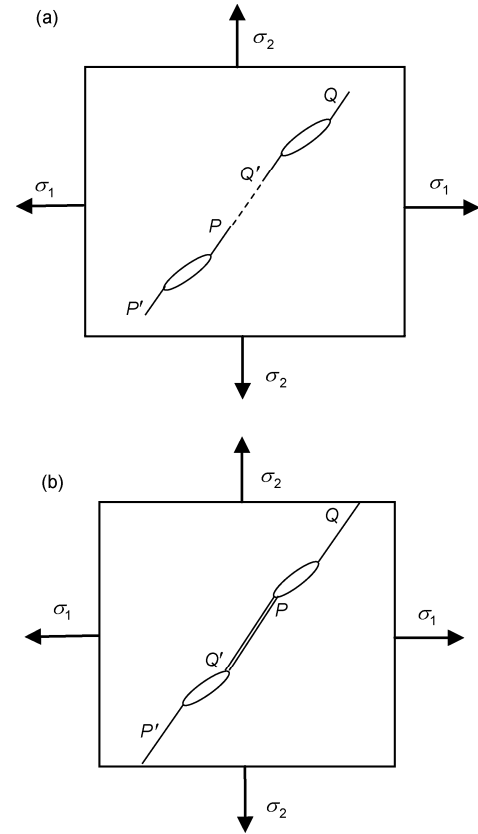

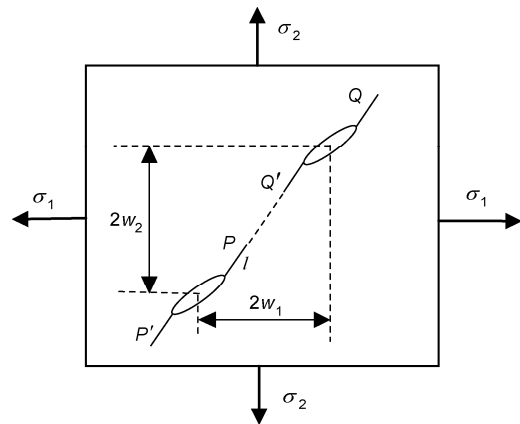**Figure 6** (a) Coalescence between two wing cracks; (b) coalescence between wing crack and initial crack.

Figure 7 Coalescence between two micro-cracks with the same direction.

where $\varepsilon^{\mathrm{cr}}_i$ is the critical strain of wing crack propagation, $\dot{\varepsilon}$ is the average strain rate, and v_{cm} is the average rate of propagation. According to Ravichandran et al. [21], v_{cm} is generally taken as $v_{cm} = (0.3 - 0.5)C_R$, where C_R is Rayleigh wave speed.

By substituting eq. (36) into eqs. (32) and (33), the failure stress σ_i^{fr} can be obtained when the coalescence occurs.

4 Results and discussion

Several researchers [24–27] did a series of experimental researches on the crack initiation, propagation and coalescence in rock materials under uniaxial and biaxial compressions, which are very helpful for us to investigate the crack-induced fracture mechanism of brittle materials. They found that open cracks are very similar to closed cracks in crack initiation, coalescence pattern and fracture process. Their results confirmed the physical significance of the micro-crack evolution and coalescence model presented in this paper. Open elliptical micro-cracks are also studied in this paper. The crack's shape (its ellipticity and size) is related to the material parameters and applied loadings; in other words, open or closed elliptical micro-cracks in the material under compression depend on the material's parameters and the loadings to which it subjects. No matter whether the micro-cracks become closed or not, at the tips of the micro-cracks wing cracks would initiate and result in fracture of the material through their coalescence.

The model of crack coalescence is directly related to the distribution of the cracks' geometric locations. Figure 8 shows the schematic diagram of three pre-existing cracks in Park and Bobet's experiments. The three cracks parallel one another. Different patterns of coalescence can be obtained by changing the spacing between the bottom right crack and the above two.

Figures 9 and 10 respectively show two modes of coalescence corresponding to two different distributions of pre-existing flaws or cracks. The length of pre-existing flaws is $2a$. The initial orientation angle is $\pi/4$. In Mode I, the spacing between two cracks in the vertical direction is $2\sqrt{2}a$, and the spacing in the horizontal direction is $\sqrt{2}a$. In Mode II, both the spacings are $\sqrt{2}a$. Through calculation it is known that these two modes are two special cases of the coalescence model of this paper. The initial orientation angle is $\beta = \pi/4$. The propagation direction of the wing crack is finally parallel to that of applied stress, that is, $\vartheta + \beta = \pi/2$. By substituting $\vartheta + \beta = \pi/2$ into eq. (34), the crack distribution condition for coalescence of wing cracks can be obtained: $w_1 = \sqrt{2}a/2$, w_2 could be arbitrary
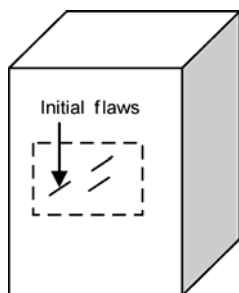

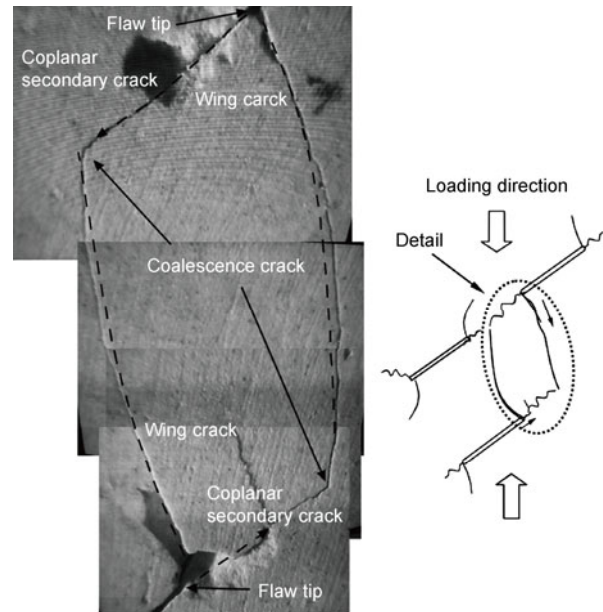**Figure 8**   Geometric location of cracks in the specimen [25].

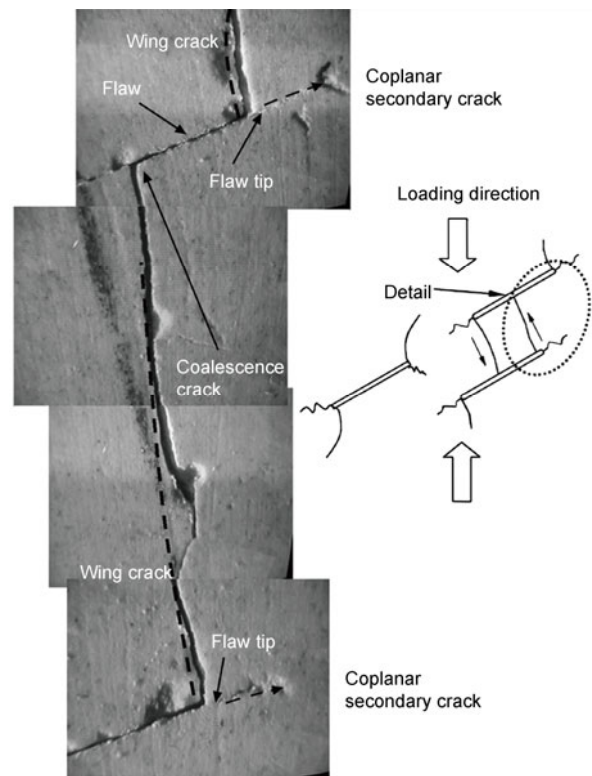**Figure 9**   Wing crack coalescence II $\left(w_1 = \sqrt{2}a/2, w_2 = \sqrt{2}a\right)$ [25].

Figure 10   Wing crack coalescence II $\left(w_1 = w_2 = \sqrt{2}a/2\right)$ [25].

value, and the wing crack propagation length depends on the value of w_2. Therefore, the micro-cracks coalescence model is consistent with the experimental results obtained by Park and Bobet.

Wong and Chau [28] did their researches on the coalescence pattern of two cracks and the strength of material under uniaxial compression. In their experiments, they

changed the relative position of two cracks and the surface friction coefficient to observe different patterns of coalescence. As a result, the patterns of crack coalescence could be classed into three modes of coalescence: (a) shear mode (coalescence between two shear cracks), (b) wing crack mode (coalescence between two wing cracks), and (c) mixed mode (mixed coalescence), as shown in Figure 11.

The wing crack mode in Figure 11(b) is in agreement with the coalescence model of this paper. The previous studies done by Park, Bobet, and Wong and Chau only qualitatively described the coalescence pattern with their experimental results, but did not give any quantitative relation between deformation and stress caused by crack coalescence. The topic on the quantitative relation between micro-crack evolution and its mechanical response will be discussed in the future study.

Theoretical results of the nonlinear constitutive model developed based on micro-crack evolution and coalescence are discussed in the following. The material parameters used in this calculation are taken from experimental results of Wong and Chau, as shown in Table 1.

The pre-existing cracks in actual materials are similar to closed cracks, meaning that their ellipticities are very small. In this paper, assume that the initial state of the material is undamaged and uniform, and in our calculation, let the ellipticity and the number density of cracks be $\rho=0.01$ and $n_a=1\times10^3$, respectively. In addition, for the stress in the case of uniaxial compression ($\sigma_2 = 0$), let $\sigma_1 = \sigma$. Using eqs. (32) and (33), the nonlinear stress-strain relations in the micro-cracks propagation can be obtained:

$$\varepsilon_1 = \left(\overline{S}_{1111} + n_a S_{11}\right)\sigma, \tag{37}$$

$$\varepsilon_2 = \left(\overline{S}_{1122} + n_a S_{12}\right)\sigma. \tag{38}$$
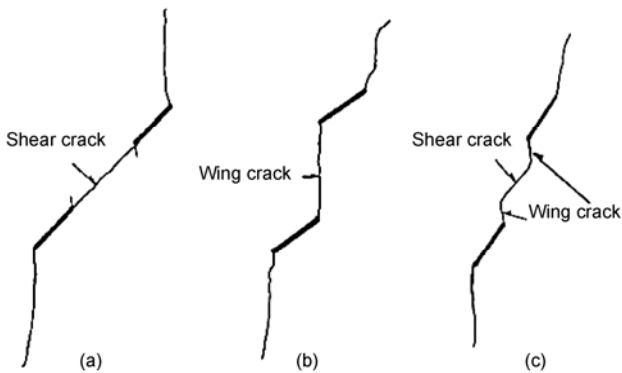

Figure 11   Three modes of crack coalescence. (a) Shear mode; (b) wing crack mode; (c) mixed mode.

Table 1   Mechanical parameters of material

E_0 (MPa)	v_0	K_{IC} $\left(MPa\cdot\sqrt{m}\right)$	$2a_0$ (mm)	$2w_1$(mm)	β
330	0.19	0.0443	12	22	$\pi/4$

In wing crack propagation, the effective elastic modulus of material is

$$E_{\text{eff}} = \frac{1}{\overline{S}_{1111} + n_a S_{11}}. \tag{39}$$

As shown in Figure 12, the effective elastic modulus of the material decreases with the wing crack propagation length increasing, though the length is very limited due to the rapidity of wing crack propagation and coalescence. Therefore, the decreasing in the elastic modulus is not obvious during the damage stage. The decreasing in the elastic modulus due to damage presents only a tiny nonlinearity in stress-strain relation. Curve (a) of Figure 13 [29] shows the actual stress-strain relation of sandstone and Curve (b) shows the stress-strain curve of uniaxial compressive modeling material used in Wong and Chau's experiments. Because the pre-existing crack is much larger than inner micro-cracks, initial mechanical properties of the material have been structurally deteriorated. Thus, the stress-strain curve of modeling material during elastic deformation stage is not linear. Curve (c) shows the computational result with the material constants of modeling material. In curve (c),
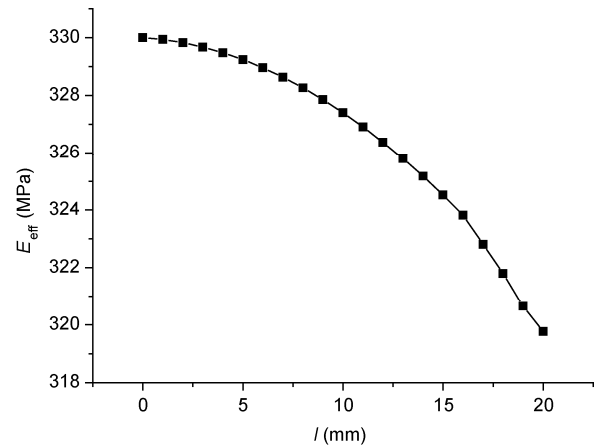

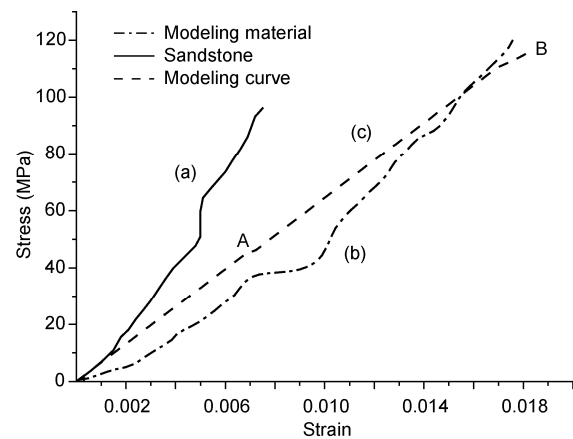**Figure 12**   Effective modulus vs. length of wing crack.

Figure 13   Stress-strain relation under uniaxial compression.

point A is the critical point, where the material starts to enter the damage stage. Because the decreasing of effective elastic modulus is very small in the damage accumulating procession, the stress-strain curve in the damage stage is almost linear. Point B is corresponding to the critical point of micro-crack coalescence. Although the material still has a larger elastic modulus during the damage process, a large number of micro-cracks coalescence makes the material fracture in a very short time. At this time the stress value describes the fracture strength of the material.

5   Conclusions

Park, Bobet, as well as Wong and Chau did similar experimental researches on the crack coalescence pattern and got basically the same law of crack coalescence, which is helpful for studying physical processes of micro-crack evolution and coalescence in some quasi-brittle materials. However, their experiments do not include the micro-crack growth law in the elastic deformation stage. This paper attempts to theoretically study the mechanical responses to the micro-crack growth, evolution, and coalescence in the materials. The constitutive model corresponding to the microstructure evolution is developed. The conclusions are as follows:

(1) Both the orientation angle and ellipticity of micro-cracks have effects on the crack growth, wing crack propagation, and coalescence, which eventually lead to formation of an anisotropic effective compliance tensor in the damaged material.

(2) The micro-crack coalescence is a highly nonlinear phenomenon which has the complicate relations to orientations, sizes, and relative positions of micro-cracks.

(3) Based on micro-crack growth, evolution, and coalescence, a constitutive model is developed and a related expression of failure strain is determined. The stress-strain relation during crack propagation stage reveals that the effective elastic modulus of damaged material decreases with increasing the wing crack propagation length.

1   Ren H L, Shu X F, Li P. Numerical and experimental investigation of the fracture behavior of shock loaded alumina. Sci China-Phys Mech Astron, 2010, 53: 244–252
2   Liu H F, Liu H Y, Song W D. Fracture characteristics of concrete subjected to impact loading. Sci China-Phys Mech Astron, 2010, 53: 253–261
3   Fanella D, Krajcinovic D. A micromechanical model for concrete in compression. Eng Fract Mech, 1988, 29: 49–66
4   Krajcinovic D, Fanella D. A micromechanical damage model for concrete. Eng Fract Mech, 1986, 25: 585–596
5   Krajcinovic D, Sumarac D. A mesomechanical model for brittle deformation processes: Part Iand II. J Appl Mech, 1989, 56: 51–62
6   Sumarac D, Krajcinovic D. A self-consistent model for microcrack-weakened solids. Mech Mater, 1897, 6: 39–52
7   Ju J W, Lee X. Micromechanical damage models for brittle solids I: Tensile loadings. J Eng Mech, 1991, 117: 1495–1514
8   Lee X, Ju J W. Micromechanical damage models for brittle solids II: Compressive loadings. J Eng Mech, 1991, 117: 1515–1536
9   Ju J W. On two-dimensional self-consistent micromechanical damage models for brittle solids. Int J Solids Struct, 1991, 27: 227–258
10   Horii H, Nemat-Nasser S. Overall moduli of solidswith microcracks: Load-induced anisotropy. J Mech Phys Solids, 1983, 31: 155–171
11   Horii H, Nemat-Nasser S. Brittle failure in compression: Splitting, faulting and brittle-ductile transition. Phil Trans Royal Soc London A, 1986, 319: 337–374
12   Yu S W, Feng X Q. A micromechanics-based damage model for microcrack-weakened brittle solids. Mech Mater, 1995, 20: 59–76
13   Feng X Q, Gross D. Micromechanical analysis of microcrack-induced residual strains in quasi-brittle solids. Comput Mater Sci, 1999, 16: 362–371
14   Kachanov M, Montague E. Interaction of a crack with certain microcrack arrays. Eng Fract Mech, 1986, 25: 625–636
15   Kachanov M, Montague E, Laures J P. Mechanics of crack-microcrack interactions. Mech Mater, 1900, 10: 59–71
16   Laures J P, Kachanov M. Three-dimensional interaction of a crack front with arrays of peny shaped microcracks. Int J Fract, 1991, 48: 255–279
17   Chudnovsky A, Dolgopolsky A, Kachanov M. Elastic interaction of a crack with a microcrack array Part I and II. Int J Solids Struct, 1987, 23: 1–21
18   Chudnovsky A, Wu S. Evaluation of energy release rate in the crack-microcrack interaction problems. Int J Solids Struct, 1992, 29: 1699–1709
19   Gong S X, Horri H. General solutions to the problems of microcracks near the tip of a main crack. J Mech Phys Solids, 1989, 37: 27–46
20   Meguid S A, Gong S X, Gaultier P E. Main crack-microcrack interaction under mode I, II and III loadings: Shielding and amplification. Int J Mech Sci, 1991, 33: 351–359
21   Ravichandran G, Subhash G. A micromecha-nical model for high strain rate behavior of ceramics. Int J Solids Struct, 1995, 32: 2627–2646
22   Wu Y Q, Huang F L. A thermal-mechanical constitutive model for b-MHX single crystal and cohesive interface under dynamic high pressure loading. Sci China-Phys Mech Astron, 2010, 53: 218–226
23   Wang Z H, Zhang Y F, Ren H L, et al. A study on compressive shock wave propagation in metallic foams. Sci China-Phys Mech Astron, 2010, 53: 279–287
24   Bobet A, Einstein H H. Fracture coalescence in rock-type materials under uniaxial and biaxial com-pression. Int J Rock Mech Mining Sci, 1998, 35: 863–888
25   Park C H, Bobet A. Crack initiation, propagation and coalescence from frictional flaws in uniaxial compression. Eng Fract Mech, 2010, 14: 2727–2748
26   Wu K T, Hao L, Wang C, et al. Level interface treatment and its application in Euler method. Sci China-Phys Mech Astron, 2010, 53: 227–236
27   Yuan K H, Qiu Z P. Nonlinear flutter analysis of stiffened composite panels in supersonic flow. Sci China-Phys Mech Astron, 2010, 53: 336–344
28   Wong R H C, Chau K T. Crack coalescence in a rock-like material containing two cracks. Int J Rock Mech Mining Sci, 1998, 35: 147–164
29   Farmer I W. Engineering Behaviour of Rocks. 2nd ed. London: Chapman & Hall, 1983